Global NEST Journal, **28** (XX), pp 1-10
Available online: 26/08/2026

Comparative evaluation of classical Fenton and UV-assisted photo-Fenton processes for the treatment of mature landfill leachate

Mohammed Azeez Othman[1], Abdulqader M. Younis[2], Bakhtyar Abdullah Othman[3], Tanya Salam Salih[4] and Reza Hashemi[5,6]*

[1]Department of Environmental Sciences and Health, College of Science, University of Salahaddin, Erbil, Kurdistan Region, Iraq. Email: mohammed.othman@su.edu.krd
[2]Department of Environmental Sciences and Health, College of Science, University of Salahaddin, Erbil, Kurdistan Region, Iraq. Email: abdulqader.younis@su.edu.krd
[3]Department of Public Health, Hawler Medical University, Kurdistan Region, Iraq. Email: bakhtiar.othman@hmu.edu.krd
[4]Department of Nutrition and Dietetics, College of Health Technology, Cihan University-Erbil, Kurdistan Region, Iraq. Email: tanya.salam@cihanuniversity.edu.iq
[5]Department of Environmental Sciences and Health, School of Public Health, Zanjan University of Medical Sciences, Zanjan, Iran. Email: reza.hashemi@hs.hmu.edu.krd
[6]Department of Nutrition and Dietetics, College of Health Sciences, Hawler Medical University, Erbil, Kurdistan Region, Iraq

*Correspondence e-mail: reza.hashemi@hs.hmu.edu.krd

Abstract

Mature landfill leachate contains refractory organic matter that limits biological treatment. This study compared classical Fenton and UV-C-assisted photo-Fenton oxidation using the same batch-reactor platform and undiluted mature leachate from the Kani-Qrzhala landfill, Erbil. Sequential factor screening evaluated pH, temperature, Fe^{2+} dose, H_2O_2 dose, reaction time and UV power. The raw leachate contained 5620 ± 380 mg L^{-1} COD, 1320 ± 45 mg L^{-1} TOC and a BOD_5/COD ratio of 0.12 ± 0.03. At the selected conditions (pH 3, 25 °C, 500 mg L^{-1} H_2O_2), classical Fenton achieved 66.3% COD removal using 300 mg L^{-1} Fe^{2+}, whereas photo-Fenton reached 90.2 ± 1.4% COD and 78.6 ± 2.3% TOC removal using 100 mg L^{-1} Fe^{2+} and 64 W UV-C. Photo-Fenton therefore used 67% less Fe^{2+}. The BMG model best described photo-Fenton kinetics (R^2 = 0.9956) and indicated a higher initial normalized degradation rate. Nominal UV energy was 128 kWh m^{-3}, emphasizing a scale-up trade-off. The results establish a site-specific performance benchmark, while multivariable optimization, toxicity/biodegradability testing, sludge characterization and pilot-scale energy validation remain necessary.

Keywords: advanced oxidation; refractory organic matter; chemical oxygen demand; total organic carbon; UV-C irradiation; sequential factor screening.

OPEN ACCESS

Received: 03/06/2026,

Accepted: 17/08/2026,

Available online: 26/08/2026

Graphical abstract

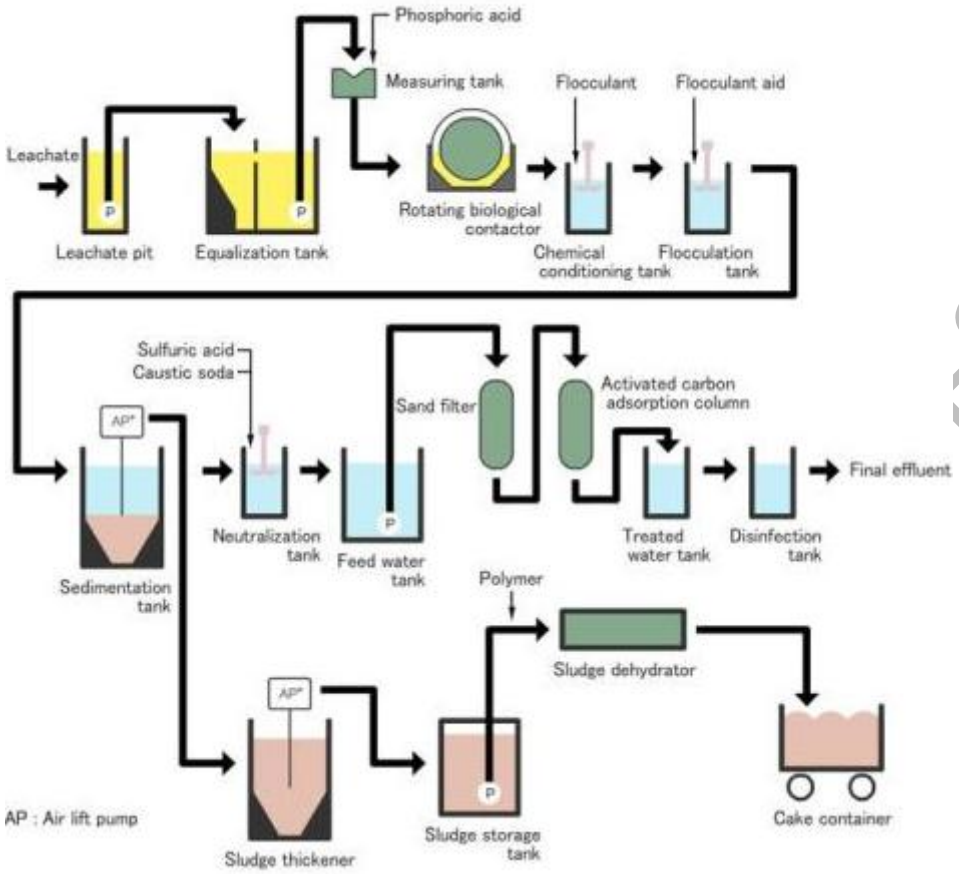

1. Introduction

Landfilling remains widely used for municipal solid waste management because of its operational simplicity and comparatively low direct cost. Its principal liquid by-product, however, is leachate: a chemically complex wastewater containing dissolved organic matter, ammoniacal nitrogen, inorganic salts and, depending on waste composition, trace organic and inorganic contaminants. Inadequately collected or treated leachate can affect soil, groundwater and receiving surface waters, making leachate management a continuing environmental priority (Kamal *et al.*, 2022; Xiang *et al.*, 2025). This concern is particularly relevant in rapidly urbanizing settings such as Erbil, where waste generation and landfill management have expanded substantially (Aziz *et al.*, 2011; Gardi, 2017; Othman, 2023).

Leachate treatability changes as a landfill ages. Young leachate generally contains a larger readily biodegradable fraction, whereas mature or stabilized leachate is enriched in humic- and fulvic-like substances and commonly exhibits a low BOD_5/COD ratio. Biological treatment alone is therefore often insufficient for old leachate, and physicochemical or advanced oxidation pretreatment may be required (Morais and Zamora, 2005; Kamal *et al.*, 2022; Rasolevandi *et al.*, 2026). Fenton oxidation is attractive in this setting because Fe^{2+} activates H_2O_2 to generate highly reactive hydroxyl radicals under acidic conditions. Its main practical constraints are strong pH dependence, peroxide scavenging at excessive doses, iron consumption, and the generation of iron-containing residual solids (Zhang *et al.*, 2005; Faggiano *et al.*, 2023).

Photo-Fenton treatment adds irradiation to the Fe/H_2O_2 system. Light can promote photoreduction of Fe(III) species to Fe(II), photodecarboxylation of ferric-organic complexes, and—particularly under UV-C—direct H_2O_2 photolysis; direct photolysis of susceptible organics and reactions mediated by dissolved organic matter may also contribute. Consequently, the performance gain under irradiation cannot automatically be attributed to a single pathway unless UV-only controls, iron speciation, or radical-scavenging experiments are available (Hermosilla *et al.*, 2009; Clemente *et al.*, 2024). Broader advanced-oxidation research likewise shows that non-Fenton energy inputs such as ultrasound can add distinct radical-generation pathways, illustrating why energy-assisted oxidation should be interpreted mechanistically rather than only by endpoint COD removal (Ahmed *et al.*, 2025).

Previous investigations have demonstrated that both conventional and photo-Fenton processes can reduce the organic load of mature leachate, but direct comparison across studies is complicated by differences in leachate composition, reactor geometry, irradiation source, reagent

ratios, pretreatment, and optimization strategy (Hermosilla *et al.*, 2009; Leszczyński, 2018; Tejera *et al.*, 2019; Charki *et al.*, 2025). Recent work has also moved beyond simple one-variable screening by applying response surface methodology (RSM), Box–Behnken or central-composite designs to quantify factor interactions, energy demand, biodegradability, sludge formation, and toxicity (Ghanbarzadeh Lak *et al.*, 2018; Faggiano *et al.*, 2023; Singa *et al.*, 2023; Grilla *et al.*, 2024; Rasolevandi *et al.*, 2026). These studies highlight two unresolved practical questions: whether the efficiency advantage of photo-Fenton persists when both processes are tested side by side on the same undiluted mature matrix, and whether the gain in organic removal is accompanied by a defensible resource trade-off rather than merely shifting burden from reagents to electrical energy.

Accordingly, this study provides a controlled bench-scale comparison of classical Fenton and UV-C-assisted photo-Fenton treatment applied to undiluted mature leachate from the Kani-Qrzhala municipal landfill in Erbil. Both processes were evaluated in the same base reactor configuration, with COD and TOC as complementary measures of oxidation and mineralization. A sequential one-factor-at-a-time (OFAT) design was used to screen pH, temperature, Fe^{2+} dose, H_2O_2 dose, reaction time and, for photo-Fenton, irradiation power. The design was chosen to isolate engineering responses with the available experimental campaign; it is not presented as a multivariable global optimization. The study therefore emphasizes reproducible local operating selections, comparative reagent demand, nominal UV-energy input, and kinetic behavior. Future work should validate these selections using multivariable designs, post-treatment biodegradability and toxicity assays, standardized sludge characterization, catalyst recovery, and continuous pilot-scale or hybrid treatment trains. Because treated-wastewater reuse and managed recharge require fit-for-purpose water quality, such downstream validation is essential before considering reuse-oriented applications (Tabieh *et al.*, 2025; Mukheef *et al.*, 2025).

2. Materials and methods

2.1. *Chemicals and reagents*

All chemicals were analytical grade and were used as received. Ferrous sulfate heptahydrate ($FeSO_4{\cdot}7H_2O$, ≥99.5%) was used as the Fe^{2+} source and hydrogen peroxide (H_2O_2, 50% w/w; Merck) as the oxidant. Concentrated H_2SO_4 (98%) and NaOH pellets were used for pH adjustment. Ultrapure water (18.2 MΩ·cm) was used to prepare analytical solutions and dilutions. COD was determined by the closed-reflux colorimetric dichromate method with Ag_2SO_4 catalysis and $HgSO_4$ for chloride interference control, in accordance with Standard Methods (APHA *et al.*, 2023).

2.2. *Leachate sampling and characterization*

Raw leachate was collected from the leachate collection pond at the Kani-Qrzhala municipal solid waste landfill, approximately 15 km from Erbil, Kurdistan Region, Iraq. The site has operated for more than 15 years and receives mixed municipal waste. Three separate field collections were made between October and December 2023 using pre-cleaned 10-L high-density polyethylene containers. Samples were immediately transported to the laboratory in an icebox, characterized on arrival, stored at 4 °C in the dark, and used within seven days. These procedures were intended to limit biological activity, photochemical alteration and volatilization during transport and storage. The three-visit window provided independent field samples for the experimental campaign but was not designed to characterize seasonal variability; therefore, the reported matrix should not be interpreted as a year-round representation of the landfill. Mature status was evaluated from landfill age and the measured low BOD_5/COD ratio, rather than by comparison with contemporaneous fresh leachate samples.

Raw-leachate characterization followed Standard Methods (APHA *et al.*, 2023). COD was measured by closed-reflux colorimetry, and TOC by high-temperature catalytic combustion with infrared detection. The reported baseline values are means ± SD from three independent field collections. Quality-control procedures included calibration curves (R^2 > 0.999), method blanks, and duplicate precision checks with deviations within ±5%.

2.3. *Experimental design and scope of optimization*

The experimental campaign used sequential OFAT screening: one factor was varied while the remaining operating conditions were held at the current selected values. This approach was used to obtain transparent, factor-specific engineering responses within a limited bench-scale campaign and to permit a direct side-by-side comparison of the two oxidation routes. Importantly, OFAT does not estimate interaction terms and may miss a different optimum arising from synergistic or antagonistic combinations of variables. Therefore, conditions identified by this design are described as 'selected conditions' or 'local optima under sequential screening', rather than as statistically proven global optima. RSM, Box–Behnken or central-composite validation is recommended before scale-up (Ghanbarzadeh Lak *et al.*, 2018; Mahtab *et al.*, 2021; Faggiano *et al.*, 2023; Rasolevandi *et al.*, 2026).

2.4. *Classical Fenton process*

Classical Fenton experiments were performed in 1-L borosilicate glass batch reactors containing 500 mL of raw leachate. The reactors were placed on a magnetic stirrer-hotplate with temperature control (±1 °C). The examined pH range was 2–5; Fe^{2+} doses were 50–400 mg L^{-1}; and H_2O_2 doses used in the dose-response experiment were 250, 500, 1000, 2000 and 3000 mg L^{-1}. After pH adjustment and Fe^{2+} addition, H_2O_2 addition defined t = 0. Mixing was maintained at 400 rpm during reagent dispersion and the initial reaction stage and then at 150 rpm. Temperature screening covered 25–40 °C, with 25 ± 1 °C retained for subsequent experiments because heating provided only a small performance gain.

2.5. *Photo-Fenton process*

Photo-Fenton experiments used the same 1-L reactor, 500-mL working volume, reagent-addition sequence and mixing

protocol as the dark process. Irradiation was supplied in a UV cabinet fitted with eight low-pressure UV-C lamps (254 nm; 8 W nominal power per lamp; 64 W total installed nominal power). Lamp combinations provided nominal powers from 16 to 64 W. A calibrated UV radiometer was used periodically to check irradiance consistency at the liquid surface, and a circulating water bath maintained the reactor at 25 ± 1 °C to separate photochemical effects from simple heating. The experimental workflow is summarized in **Figure 1**.

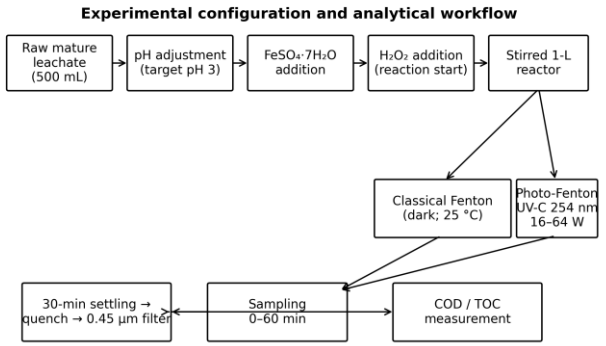

Figure 1. Bench-scale workflow used for the side-by-side classical Fenton and UV-C-assisted photo-Fenton experiments. The same base reactor and 500-mL working volume were used for both routes; UV-C irradiation was applied only in the photo-Fenton branch.

2.6. *Reaction-time sampling and analytical methods*

Aliquots were withdrawn at 0, 10, 20, 30, 40, 50 and 60 min to capture the rapid initial oxidation stage and the subsequent approach toward a plateau within the pre-specified 60-min experimental window. After each run, the reaction mixture was allowed to settle for approximately 30 min. The clarified phase was then quenched, filtered through a 0.45-µm PTFE membrane and analyzed. No validated samples were collected at 120 min; consequently, the manuscript does not extrapolate or claim behavior at two hours. Longer-duration kinetics should be evaluated in future studies if persistent tailing or delayed mineralization is of interest.

Residual H_2O_2 was quenched before COD digestion because peroxide can consume dichromate and produce a positive analytical bias in the standard COD test (Kang *et al.*, 1999). After quenching and 0.45-µm filtration, COD and TOC were measured as described above. Each experimental condition comprised three independent runs; duplicate analytical determinations within each run were averaged first, and the resulting run-level values were used to calculate the reported mean and SD. The limits of detection were 10 mg L^{-1} for COD and 0.5 mg L^{-1} for TOC. Removal efficiency was calculated as: $\eta\ (\%) = [(C_o - C_t)/C_o] \times 100$, where C_o is the initial concentration and C_t is the concentration at reaction time t. This mass-balance expression is widely used in Fenton leachate studies (Zhang *et al.*, 2005; Faggiano *et al.*, 2023).

2.7. *Kinetic modeling*

COD-time data were fitted to zero-order, pseudo-first-order, pseudo-second-order and Behnajady–Modirshahla–Ghanbary (BMG) models in OriginPro 2022. For the BMG formulation, $t/(1 - C_t/C_o) = m + bt$; 1/m represents the model-derived initial normalized degradation rate and 1/b the theoretical maximum fractional removal represented by the fitted curve (Behnajady *et al.*, 2007). Model performance was compared using R^2, with residual patterns inspected as an additional diagnostic. Because the BMG model is empirical, its parameters were interpreted as comparative descriptors of the observed biphasic kinetics rather than as elementary chemical rate constants.

2.8. *Statistical analysis*

Results are presented as mean ± SD from three independent runs per condition. One-way ANOVA followed by Tukey's HSD test was used for comparisons among levels of a single screened factor (SPSS version 27), with two-sided $p < 0.05$ considered statistically significant. Before parametric inference, residual and normal-probability plots were inspected for gross deviations from normality and residual-versus-fitted plots were inspected for marked variance heterogeneity. Given the small number of independent runs per condition (n = 3), formal normality tests were not over-interpreted. To improve statistical transparency, the analysis reports t-based 95% confidence intervals for key final outcomes, the absolute between-process difference, and ANOVA F statistics with η^2 effect sizes for the Fe^{2+}- and H_2O_2-dose experiments. No interaction term is reported because the sequential OFAT design does not support valid estimation of multivariable interactions.

3. Results

3.1. *Characteristics of raw landfill leachate*

The raw leachate had high organic strength and low biodegradability (**Table 1**). Mean COD and TOC were 5620 ± 380 and 1320 ± 45 mg L^{-1}, respectively, while BOD_5/COD was 0.12 ± 0.03. Conductivity (25.6 ± 3.2 mS cm^{-1}) and NH_3-N (1480 ± 120 mg L^{-1}) further indicate a concentrated mature matrix. These baseline characteristics define the matrix tested in this study; they should not be generalized to other seasons or landfills without additional sampling.

Table 1. Initial physicochemical characteristics of Kani-Qrzhala mature landfill leachate (mean ± SD, n = 3 independent field collections).

Parameter	Unit	Value
pH	–	7.8 ± 0.4
COD	mg L^{-1}	5620 ± 380
TOC	mg L^{-1}	1320 ± 45
BOD_5/COD	–	0.12 ± 0.03
Conductivity	mS cm^{-1}	25.6 ± 3.2
NH_3-N	mg L^{-1}	1480 ± 120

Table 2. Effect of Fe^{2+} dose on COD and TOC removal (pH 3.0, H_2O_2 = 2000 mg L^{-1}, 25 °C; classical Fenton = 50 min, photo-Fenton = 60 min; mean ± SD, n = 3 independent runs).

Fe^{2+} (mg L^{-1})	Classical COD (%)	Classical TOC (%)	Photo-Fenton COD (%)	Photo-Fenton TOC (%)
50	38.2 ± 2.1	32.4 ± 1.8	71.5 ± 2.3	58.7 ± 2.1
100	51.7 ± 1.9	47.9 ± 2.0	82.1 ± 2.4	71.3 ± 2.5
200	57.4 ± 2.3	53.1 ± 1.7	79.8 ± 1.9	68.4 ± 2.0
300	60.4 ± 1.8	55.6 ± 2.2	75.2 ± 2.1	64.9 ± 1.8
400	58.9 ± 2.0	53.8 ± 1.9	71.6 ± 2.4	60.2 ± 2.3

3.2. *Sequential screening of pH and temperature*

Both oxidation routes were strongly pH dependent. The selected pH was 3.0, consistent with the acidic range that maintains catalytically active iron species and effective peroxide activation. At pH 3.0, the screening experiment reported COD removal of 48.2 ± 1.9% for classical Fenton (300 mg L^{-1} Fe^{2+} and 2000 mg L^{-1} H_2O_2) and 71.4 ± 2.3% for photo-Fenton (100 mg L^{-1} Fe^{2+}, the same H_2O_2 dose and 64 W UV-C). Photo-Fenton also retained high removal at pH 2.5 (68.9%), whereas performance declined outside the acidic operating window. Accordingly, pH 3.0 was retained for the subsequent dose-response and time experiments.

Temperature had a comparatively small effect over the tested 25–40 °C range. Raising the temperature from 25 to 40 °C increased COD removal by only approximately 3–4 percentage points in classical Fenton and by less in the irradiated system. The selected temperature was therefore 25 °C, avoiding deliberate heat input. Accordingly, 25 °C was retained for subsequent experiments to avoid unnecessary heat input.

3.3. *Fe^{2+} dose response*

Fe^{2+} dose had a large effect in both processes (**Table 2**; **Figure 2**). In classical Fenton, COD removal increased to 60.4 ± 1.8% at 300 mg L^{-1} Fe^{2+}, with little additional benefit at 400 mg L^{-1}. In photo-Fenton, the highest COD removal in the Fe^{2+} screen occurred at 100 mg L^{-1} (82.1 ± 2.4%), after which performance declined. The selected catalyst doses were therefore 300 mg L^{-1} for classical Fenton and 100 mg L^{-1} for photo-Fenton. This represents a 67% reduction in the applied Fe^{2+} dose for the irradiated route. The one-way dose effects were large (η^2 = 0.960 for classical COD and 0.847 for photo-Fenton COD; **Table 5**).

Table 3. Effect of H_2O_2 dose on COD and TOC removal (pH 3.0, 25 °C; classical Fenton Fe^{2+} = 300 mg L^{-1}; photo-Fenton Fe^{2+} = 100 mg L^{-1}; mean ± SD, n = 3 independent runs).

H_2O_2 (mg L^{-1})	Classical COD (%)	Classical TOC (%)	Photo-Fenton COD (%)	Photo-Fenton TOC (%)
3000	59.8 ± 2.4	56.2 ± 2.1	78.5 ± 2.0	64.7 ± 1.9
2000	60.1 ± 1.7	58.4 ± 1.8	82.3 ± 1.6	70.1 ± 2.2
1000	52.3 ± 2.2	48.7 ± 2.0	84.7 ± 2.3	72.8 ± 1.7
500	66.3 ± 1.6	62.1 ± 1.5	86.4 ± 2.1	74.9 ± 2.0
250	54.7 ± 1.9	51.3 ± 2.3	79.2 ± 1.8	68.5 ± 2.1

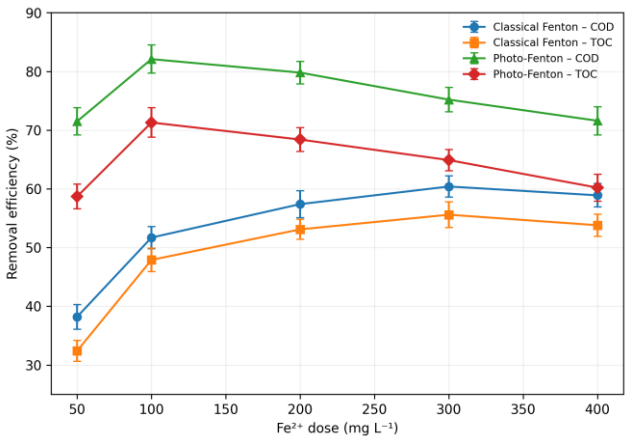

Figure 2. Effect of Fe^{2+} dose on COD and TOC removal. Points are means and error bars are SD (n = 3 independent runs). Numerical values correspond exactly to **Table 2**.

3.4. *H_2O_2 dose response*

The H_2O_2 dose-response was non-monotonic (**Table 3**; **Figure 3**). At the selected Fe^{2+} doses, 500 mg L^{-1} H_2O_2 gave the highest reported COD removal in both systems: 66.3 ± 1.6% for classical Fenton and 86.4 ± 2.1% for photo-Fenton. TOC removal at the same H_2O_2 level was 62.1 ± 1.5% and 74.9 ± 2.0%, respectively. Higher peroxide doses did not improve removal, consistent with the well-known competition between productive radical generation and scavenging/self-decomposition when H_2O_2 is excessive. The H_2O_2-dose effect was also large (η^2 = 0.900 for classical COD and 0.782 for photo-Fenton COD; **Table 5**).

3.5. *Reaction time and final process comparison*

Within the 0–60 min experimental window, classical Fenton reached 66.3% COD removal at 50 min, with no statistically significant improvement reported by 60 min (p = 0.42). Photo-Fenton continued to improve to 60 min and reached 90.2 ± 1.4% COD removal and 78.6 ± 2.3% TOC removal. Accordingly, 50 and 60 min were retained as the selected reaction times for classical and photo-Fenton treatment, respectively. The absolute difference in final COD removal was 23.9 percentage points (95% CI for the difference, 20.5–27.3 percentage points, calculated from the reported summary statistics). **Figure 4** provides a direct endpoint comparison. No data beyond 60 min were collected, so longer-term behavior should be established experimentally rather than extrapolated.

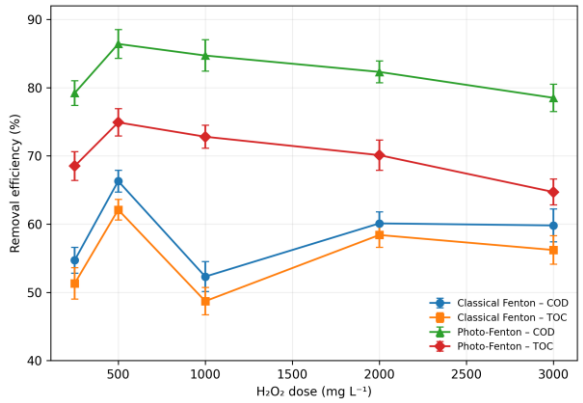

Figure 3. Effect of H_2O_2 dose on COD and TOC removal. Points are means and error bars are SD (n = 3 independent runs). Numerical values correspond exactly to **Table 3**.

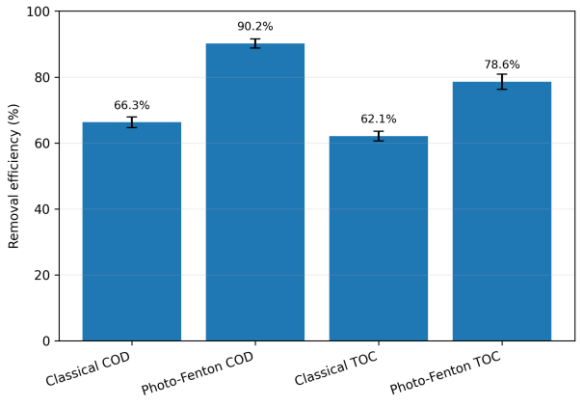

Figure 4. Final COD and TOC removal under the selected process conditions. Bars are means and error bars are SD (n = 3 independent runs).

3.6. *Effect of UV-C power and nominal energy demand*

For photo-Fenton, increasing nominal lamp power from 16 to 64 W increased COD removal from approximately 71% to 90.2%, with the reported power-response relationship $R^2 = 0.978$. At 64 W and 60 min, residual H_2O_2 was reported as below the analytical detection limit. At this condition, nominal lamp-energy input was 64 W × 1 h = 0.064 kWh for the 0.5-L batch, corresponding to 0.128 kWh L^{-1}, or 128 kWh m^{-3}, based solely on nominal lamp power. This is a substantial bench-scale energy intensity and should not be interpreted as evidence of full-scale economic feasibility. It excludes mixing, cooling and ancillary energy and is used only as a transparent screening metric.

Table 4 integrates the selected operating conditions and resource intensities. Using the mean initial COD of 5620 mg L^{-1}, the reported removal percentages correspond to calculated mean residual COD concentrations of approximately 1894 mg L^{-1} after classical Fenton and 551 mg L^{-1} after photo-Fenton. These final concentrations are derived from the mean baseline COD and mean removal percentage; they are not independent direct measurements with separately estimated SDs. The comparison therefore shows the principal trade-off clearly: photo-Fenton produced greater organic removal with one-third of the Fe^{2+} dose, but required UV-C electricity and a longer selected reaction time.

Table 4. Selected operating conditions, endpoint performance and screening-level resource intensity. Final COD/TOC concentrations marked "calculated" were obtained from the mean initial concentration × (1 − mean removal fraction) and are provided for transparent comparison, not as independently measured endpoints.

Metric	Classical Fenton	Photo-Fenton
Initial COD	5620 ± 380 mg L^{-1}	5620 ± 380 mg L^{-1}
COD removal	66.3 ± 1.6% (95% CI 62.3–70.3)	90.2 ± 1.4% (95% CI 86.7–93.7)
Final COD (calculated)	≈1894 mg L^{-1}	≈551 mg L^{-1}
Initial TOC	1320 ± 45 mg L^{-1}	1320 ± 45 mg L^{-1}
TOC removal	62.1 ± 1.5% (95% CI 58.4–65.8)	78.6 ± 2.3% (95% CI 72.9–84.3)
Final TOC (calculated)	≈500 mg L^{-1}	≈282 mg L^{-1}
pH / temperature	3.0 / 25 °C	3.0 / 25 °C
Fe^{2+} dose	300 mg L^{-1}	100 mg L^{-1}
H_2O_2 dose	500 mg L^{-1}	500 mg L^{-1}
Selected reaction time	50 min	60 min
UV-C nominal power	0 W	64 W
Nominal lamp energy	0	0.128 kWh L^{-1} (128 kWh m^{-3})
Key unquantified burdens	Acid/base; residual iron; sludge handling	Acid/base; lamp/maintenance; residual iron; sludge handling

Table 5. Summary-statistic one-way ANOVA results for the Fe^{2+}- and H_2O_2-dose experiments (n = 3 per level). F and η^2 were calculated from the reported group means and SDs; η^2 is the proportion of total variance attributable to the screened dose factor.

Factor	Outcome	df (between, within)	F	p	η^2
Fe^{2+} dose	Classical COD	4, 10	60.06	<0.001	0.960
Fe^{2+} dose	Classical TOC	4, 10	72.50	<0.001	0.967
Fe^{2+} dose	Photo-Fenton COD	4, 10	13.88	<0.001	0.847
Fe^{2+} dose	Photo-Fenton TOC	4, 10	18.36	<0.001	0.880
H_2O_2 dose	Classical COD	4, 10	22.48	<0.001	0.900
H_2O_2 dose	Classical TOC	4, 10	22.71	<0.001	0.901
H_2O_2 dose	Photo-Fenton COD	4, 10	8.96	0.002	0.782
H_2O_2 dose	Photo-Fenton TOC	4, 10	11.77	<0.001	0.825

3.7. *Kinetic modeling*

The kinetic comparison is summarized in **Table 6**. The BMG model provided the highest R^2 for photo-Fenton (0.9956) and a better description of its biphasic profile than the simpler tested models. For classical Fenton, the BMG R^2 was 0.9489, exceeding the corresponding zero-order, pseudo-first-order and pseudo-second-order fits. The fitted BMG m parameter was lower for photo-Fenton (10.447) than for classical Fenton (24.107). The corresponding 1/m values were 0.0957 and 0.0415 min^{-1}, indicating an approximately 2.3-fold larger model-derived initial normalized degradation rate under irradiation. The derived 1/b values were 0.774 and 0.676, respectively. These empirical parameters support faster early oxidation in the irradiated system but do not by themselves identify the responsible radical pathway.

4. Discussion

Table 6. Kinetic parameters and goodness-of-fit for classical and photo-Fenton processes. For BMG, 1/m is the model-derived initial normalized degradation rate and 1/b is the theoretical maximum fractional removal represented by the fitted model.

Model / parameter	Classical Fenton	Photo-Fenton
Zero-order: k_o (mg L^{-1} min^{-1}); R^2	23.62; 0.9005	20.56; 0.9718
Pseudo-first-order: k_1 (min^{-1}); R^2	0.0090; 0.8805	0.0109; 0.9896
Pseudo-second-order: k_2 (L mg^{-1} min^{-1}); R^2	6.0×10^{-6}; 0.8526	6.0×10^{-8}; 0.9842
BMG: m; b; R^2	24.107; 1.479; 0.9489	10.447; 1.292; 0.9956
BMG-derived 1/m (min^{-1})	0.0415	0.0957
BMG-derived 1/b (fraction)	0.676	0.774

The distinction between COD removal and mineralization is important. At the final photo-Fenton condition, COD removal (90.2%) exceeded TOC removal (78.6%) by 11.6 percentage points. This difference indicates that a portion of the original oxidizable load was transformed without complete conversion of organic carbon to CO_2. Plausible products during Fenton oxidation include lower-molecular-weight carboxylic acids, partially oxidized aromatics, aldehydes and other oxygenated intermediates, but the present study did not perform chromatographic identification and therefore cannot assign specific transformation products. Incomplete mineralization can either increase biodegradability by fragmenting refractory molecules or, in some matrices, transiently generate inhibitory intermediates. Studies that directly measured BOD_5/COD or ecotoxicity demonstrate why these endpoints must be evaluated rather than inferred from COD alone (Morais and Zamora, 2005; Colombo *et al.*, 2019; Grilla *et al.*, 2024; Rasolevandi *et al.*, 2026). Accordingly, COD and TOC endpoints alone do not demonstrate improved downstream biodegradability or reduced toxicity.

The UV enhancement is mechanistically compatible with several simultaneous pathways. Photoreduction of Fe(III)-hydroxo and ferric-organic complexes can regenerate Fe^{2+} and sustain Fenton cycling; UV-C can also photolyze H_2O_2 directly, while susceptible chromophores or dissolved organic matter may undergo direct or sensitized photochemistry. The lower selected Fe^{2+} dose and larger BMG-derived initial normalized rate under irradiation are consistent with more effective radical production, but they do not distinguish among these mechanisms. Without UV-only controls, radical-scavenger experiments, ferric/ferrous speciation, photon-flux-normalized kinetics, or transformation-product analysis, the relative contribution of catalyst regeneration versus Fe-independent photochemical oxidation cannot be quantified. We therefore frame the mechanistic explanation as supported interpretation rather than proof (Hermosilla *et al.*, 2009; Clemente *et al.*, 2024; Charki *et al.*, 2025).

The pH and reagent-dose behavior is chemically plausible but the sequential design imposes an important boundary on the meaning of 'optimum'. RSM studies of leachate treatment have demonstrated meaningful interactions among pH, iron, peroxide, reaction time and energy input (Ghanbarzadeh Lak *et al.*, 2018; Mahtab *et al.*, 2021; Faggiano *et al.*, 2023; Singa *et al.*, 2023). In the present OFAT campaign, each selected level is therefore a local engineering choice conditional on the levels fixed at that step. A different combination could yield a higher removal efficiency, lower energy demand or lower chemical burden. Accordingly, multivariable validation is a priority before any pilot-scale design.

The resource comparison also changes the practical interpretation of photo-Fenton. A 67% reduction in applied Fe^{2+} can reduce chemical use and may reduce the potential for iron-rich residual solids, but actual sludge yield, composition, iron content, dewaterability and disposal properties were not characterized using a standardized

protocol in the validated dataset. Because standardized sludge measurements were not available, no quantitative sludge-reduction value is reported. Recent work has shown that sludge-to-iron and organic-removal-to-sludge indices can be incorporated directly into Fenton optimization (Faggiano *et al.*, 2023), and detailed solid-phase characterization has also been reported for Fenton-family treatments (Singa *et al.*, 2023). These approaches should be included in a follow-up study together with residual dissolved iron and catalyst-recovery measurements.

Likewise, the nominal UV energy of 128 kWh m^{-3} is not minor. Photo-Fenton can outperform the dark process chemically, but at this bench scale the gain is accompanied by a high volumetric electrical input. Energy-optimized RSM studies show that COD removal and photo-energy demand should be optimized jointly rather than maximizing lamp power alone (Ghanbarzadeh Lak *et al.*, 2018). Solar photo-Fenton, improved optical path length, higher irradiated volume per lamp, lamp efficiency, staged irradiation, and integration with complementary treatment steps are potential routes to lower energy intensity (Clemente *et al.*, 2024). Consequently, 64 W is best described as the highest-performing tested bench-scale level—not an economically proven full-scale optimum.

A screening-level resource balance (**Table 4**) further shows why lower iron demand cannot be equated with lower total cost. Both selected routes used 500 mg L^{-1} H_2O_2 and required acidification to approximately pH 3 followed by neutralization before discharge or biological treatment. Photo-Fenton additionally requires irradiation hardware, lamp replacement, electrical power and optical maintenance; the classical route applies more iron and may impose a larger solids-management burden. Market-price-based costing was not attempted because local bulk chemical and electricity prices, reactor depreciation and sludge-disposal costs were not part of the dataset. This avoids a false-precision economic estimate. For context, recent hybrid Fenton–membrane work has demonstrated that meaningful cost evaluation requires explicit accounting of operating configuration and toxicity of the treated effluent (Torres *et al.*, 2025).

Residual oxidant is another integration issue. Under the final 64-W photo-Fenton condition, residual H_2O_2 was below the analytical detection limit after 60 min, but this observation should not be generalized to all operating conditions or to the dark process. Peroxide must be quenched before COD analysis to prevent positive bias (Kang *et al.*, 1999), and any residual oxidant entering a biological unit may inhibit microorganisms or distort oxygen-demand measurements. Full treatment-train studies should therefore measure residual H_2O_2 and dissolved iron immediately before biological polishing and define a reproducible quenching/neutralization step.

Scale-up introduces additional limitations beyond nominal energy. Mature leachate is optically dense, so UV penetration and reactor hydrodynamics can become limiting as path length increases. Continuous flow, reagent dosing, mixing, heat management, lamp fouling, solids separation and safe handling of H_2O_2 must also be engineered. Pilot evidence shows that performance can decrease from laboratory to larger scale even when nominal conditions are held constant, reinforcing the need for scale-specific validation (Grilla *et al.*, 2024). Hybrid arrangements that pair oxidation with biological or membrane processes may be more realistic than stand-alone oxidation when discharge or reuse standards require removal of residual organics, nitrogen, toxicity and solids (Colombo *et al.*, 2019; Torres *et al.*, 2025).

Finally, the use of real leachate is a strength for matrix realism but also limits external validity. All samples came from one landfill and from an October–December 2023 campaign. Landfill age, waste composition, rainfall, temperature, dilution, recirculation and operational history can alter organic matter, ammonia, alkalinity, salinity and radical-scavenging capacity. The present findings therefore establish a rigorous site-specific benchmark rather than a universal process recipe. Seasonal sampling and paired evaluation of fresh versus mature leachate would be valuable, as recent work has shown that leachate age can materially change both pretreatment requirements and biodegradability response (Rasolevandi *et al.*, 2026).

5. Study limitations

The study should be interpreted within five principal constraints: (i) the sequential OFAT design does not estimate factor interactions or prove a global optimum; (ii) the experimental matrix represents one mature landfill and a limited sampling window; (iii) post-treatment BOD_5/COD, ecotoxicity, transformation products, residual dissolved iron, and standardized sludge properties were not measured; (iv) the highest-performing UV condition required a substantial nominal bench-scale energy input (128 kWh m^{-3} based on lamp power alone); and (v) the batch reactor does not reproduce continuous-flow hydraulics, light attenuation, fouling, or full treatment-train operation. Accordingly, the conclusions are deliberately restricted to endpoints supported by the available measurements.

6. Conclusions

In undiluted mature Kani-Qrzhala leachate, UV-C-assisted photo-Fenton treatment provided a clear oxidation advantage over classical Fenton under the sequentially selected bench-scale conditions. At pH 3 and 25 °C with 500 mg L^{-1} H_2O_2, classical Fenton achieved 66.3% COD removal using 300 mg L^{-1} Fe^{2+} and a 50-min selected reaction time, whereas photo-Fenton reached 90.2% COD and 78.6% TOC removal using 100 mg L^{-1} Fe^{2+}, 64 W UV-C and 60 min. The irradiated route therefore reduced the applied Fe^{2+} dose by 67% and exhibited a larger BMG-derived initial normalized degradation rate. The benefit, however, is accompanied by a nominal UV-energy intensity of 128 kWh m^{-3} at the 0.5-L bench scale. The study consequently supports photo-Fenton as a technically effective oxidation route, but not yet as an economically or environmentally proven full-scale solution. Multivariable optimization, seasonal validation, post-treatment biodegradability and toxicity testing, residual iron and peroxide control, standardized sludge

characterization, catalyst recovery, pilot-scale continuous operation and life-cycle/techno-economic assessment are required before implementation in a hybrid treatment train.

Acknowledgements

The authors gratefully acknowledge the technical support provided by the Environmental Research Laboratory at the College of Science, University of Salahaddin-Erbil, and the landfill management office in Erbil Municipality for facilitating leachate sampling.

Declaration of generative AI and AI-assisted technologies

During revision, AI-assisted software was used for language editing, editorial organization and calculation checking based on the authors' reported summary data. No experimental observations were generated or altered. The authors reviewed the final text, numerical calculations, references and interpretations and take full responsibility for the content.

Conflict of interest

The authors declare that they have no known competing financial interests or personal relationships that could have appeared to influence the work reported in this paper.

Author contributions

Mohammed Azeez Othman: Conceptualization, Methodology, Investigation, Data curation, Formal analysis, Visualization, Writing – original draft. Abdulqader M. Younis: Investigation, Methodology, Formal analysis, Validation, Writing – review & editing. Bakhtyar Abdullah Othman: Resources, Validation. Tanya Salam Salih: Resources, Validation. Reza Hashemi: Conceptualization, Supervision, Project administration, Validation, Writing – review & editing. All authors read and approved the final version of the manuscript.

Funding

This research did not receive any specific grant from funding agencies in the public, commercial, or not-for-profit sectors.

Ethics approval and consent to participate

Not applicable. This study involved only chemical and physicochemical analyses of landfill leachate samples and did not include human participants or animal subjects.

Consent for publication

Not applicable.

Availability of data and materials

The datasets generated and/or analyzed during the current study are available from the corresponding author upon reasonable request.

References

Ahmed, M.E., Khajah, M., Abdullah, H. and Al-Yaseen, R. (2025), Treatment of industrial wastewater of variable quality using ultrasound irradiation, Civil Engineering Journal, 11(4), 1476–1491. https://doi.org/10.28991/CEJ-2025-011-04-013.

APHA, AWWA and WEF (2023), Standard Methods for the Examination of Water and Wastewater, 24th ed., APHA Press, Washington, DC.

Aziz, S.Q., Aziz, H.A., Bashir, M.J.K. and Yusoff, M.S. (2011), Appraisal of domestic solid waste generation, components, and the feasibility of recycling in Erbil, Iraq, Waste Management & Research, 29, 880–887.

Behnajady, M.A., Modirshahla, N. and Ghanbary, F. (2007), A kinetic model for the decolorization of C.I. Acid Yellow 23 by Fenton process, Journal of Hazardous Materials, 148, 98–102. https://doi.org/10.1016/j.jhazmat.2007.02.003.

Charki, A., Fraiha, O., Zaki, N., Hadoudi, N. and El Ouarghi, H. (2025), Advanced oxidation of synthetic leachate: Performance of the photo-Fenton process for COD removal, Results in Chemistry, 18, 102827. https://doi.org/10.1016/j.rechem.2025.102827.

Clemente, E., Domingues, E., Quinta-Ferreira, R.M., Leitão, A. and Martins, R.C. (2024), Solar photo-Fenton and persulphate-based processes for landfill leachate treatment: A critical review, Science of the Total Environment, 912, 169471. https://doi.org/10.1016/j.scitotenv.2023.169471.

Colombo, A., Módenes, A.N., Góes Trigueros, D.E., Giordani da Costa, S.I., Borba, F.H. and Espinoza-Quiñones, F.R. (2019), Treatment of sanitary landfill leachate by the combination of photo-Fenton and biological processes, Journal of Cleaner Production, 214, 145–153. https://doi.org/10.1016/j.jclepro.2018.12.310.

Faggiano, A., De Carluccio, M., Cerrato, F., Garcia Junior, C.A., Proto, A., Fiorentino, A. and Rizzo, L. (2023), Improving organic matter and nutrients removal and minimizing sludge production in landfill leachate pre-treatment by Fenton process through a comprehensive response surface methodology approach, Journal of Environmental Management, 340, 117950. https://doi.org/10.1016/j.jenvman.2023.117950.

Gardi, S.Q.S. (2017), Environmental impact assessment of Erbil dumpsite area-West of Erbil City-Iraqi Kurdistan Region, Journal of Tethys, 5, 194–217.

Ghanbarzadeh Lak, M., Sabour, M.R., Ghafari, E. and Amiri, A. (2018), Energy consumption and relative efficiency improvement of photo-Fenton – Optimization by RSM for landfill leachate treatment, a case study, Waste Management, 79, 58–70. https://doi.org/10.1016/j.wasman.2018.07.029.

Grilla, E., Parthenidis, P., Filiou, A., Isari, E., Gkouvousis, P., Kokkinos, P., Papaioannou, D., Evgenidou, E., Lambropoulou, D.A. and Kalavrouziotis, I.K. (2024), Phytotoxicity and ecotoxicity assessment of landfill leachate treated by UV-Fenton: From lab to pilot scale, Sustainable Chemistry and Pharmacy, 38, 101483. https://doi.org/10.1016/j.scp.2024.101483.

Hermosilla, D., Cortijo, M. and Huang, C.P. (2009), Optimizing the treatment of landfill leachate by conventional Fenton and photo-Fenton processes, Science of the Total Environment, 407, 3473–3481. https://doi.org/10.1016/j.scitotenv.2009.02.009.

Kamal, A., Makhatova, A., Yergali, B., Baidullayeva, A., Satayeva, A., Kim, J., Inglezakis, V.J., Poulopoulos, S.G. and Arkhangelsky, E. (2022), Biological treatment, advanced oxidation and membrane separation for landfill leachate treatment: A review, Sustainability, 14, 14427. https://doi.org/10.3390/su142114427.

Kang, Y.W., Cho, M.J. and Hwang, K.Y. (1999), Correction of hydrogen peroxide interference on standard chemical oxygen demand test, Water Research, 33, 1247–1251. https://doi.org/10.1016/S0043-1354(98)00315-7.

Leszczyński, J. (2018), Treatment of landfill leachate by using Fenton and photo-Fenton processes, Journal of Ecological Engineering, 19(5), 194–199. https://doi.org/10.12911/22998993/89824.

Mahtab, M.S., Islam, D.T. and Farooqi, I.H. (2021), Optimization of the process variables for landfill leachate treatment using Fenton based advanced oxidation technique, Engineering Science and Technology, an International Journal, 24, 428–435. https://doi.org/10.1016/j.jestch.2020.08.013.

Morais, J.L. and Zamora, P.P. (2005), Use of advanced oxidation processes to improve the biodegradability of mature landfill leachates, Journal of Hazardous Materials, 123, 181–186. https://doi.org/10.1016/j.jhazmat.2005.03.041.

Mukheef, R.A.H., Hassan, W.H. and Alquzweeni, S. (2025), Artificial recharge of an unconfined aquifer using treated wastewater as a climate change mitigation strategy, Civil Engineering Journal, 10, 319–343. https://doi.org/10.28991/CEJ-SP2024-010-016.

Othman, M.A. (2023), Treatment of leachate from Erbil landfill site by electro- and chemical coagulation methods, Science Journal of University of Zakho, 11(4), 557–563. https://doi.org/10.25271/sjuoz.2023.11.4.1181.

Primo, O., Rivero, M.J. and Ortiz, I. (2008), Photo-Fenton process as an efficient alternative to the treatment of landfill leachates, Journal of Hazardous Materials, 153, 834–842. https://doi.org/10.1016/j.jhazmat.2007.09.053.

Rasolevandi, T., Naddafi, K., Hassanvand, M.S., Hadi, M., Alimohammadi, M. and Yaghmaeian, K. (2026), Feasibility study on enhancing the biodegradability of fresh and old landfill leachate using combined chemical precipitation and Fenton processes, Scientific Reports, 16, 14154. https://doi.org/10.1038/s41598-026-42622-9.

Singa, P.K., Isa, M.H., Baskaran, S., Ho, Y.C., Lim, J.W. and Rajamohan, N. (2023), PAHs remediation from hazardous waste landfill leachate using Fenton, photo-Fenton and electro-Fenton oxidation processes: Performance evaluation under optimized conditions using RSM and ANN, Environmental Research, 231, 116191. https://doi.org/10.1016/j.envres.2023.116191.

Tabieh, M.A., Al-Karablieh, E.K., Qtaishat, T.H., Salman, A.Z., Thaher, N.H., Al-Karablieh, N.K., Al-Jaghbir, M.T., Al-Zghoul, T.M. and Jamrah, A.I. (2025), Assessment of fresh water reallocation by treated wastewater for irrigation, HighTech and Innovation Journal, 6(1), 236–256. https://doi.org/10.28991/HIJ-2025-06-01-016.

Tejera, J., Miranda, R., Hermosilla, D., Urra, I., Negro, C. and Blanco, A. (2019), Treatment of a mature landfill leachate: Comparison between homogeneous and heterogeneous photo-Fenton with different pretreatments, Water, 11, 1849. https://doi.org/10.3390/w11091849.

Torres, R.C., de Almeida, R., Fonseca, F.V. and Campos, J.C. (2025), Cost-effective treatment of landfill leachate using Fenton oxidation and submerged microfiltration: Comparison of the two-stage and simultaneous configurations, Journal of Environmental Chemical Engineering, 13, 119282. https://doi.org/10.1016/j.jece.2025.119282.

Xiang, R., Wei, W., Mei, T., Wei, Z., Yang, X., Liang, J. and Zhu, J. (2025), A review on landfill leachate treatment technologies: Comparative analysis of methods and process innovation, Applied Sciences, 15, 3878. https://doi.org/10.3390/app15073878.

Zazouli, M.A., Yousefi, Z., Eslami, A. and Ardebilian, M.B. (2012), Municipal solid waste landfill leachate treatment by Fenton, photo-Fenton and Fenton-like processes: Effect of some variables, Journal of Environmental Health Science and Engineering, 9, 3. https://doi.org/10.1186/1735-2746-9-3.

Zhang, H., Choi, H.J. and Huang, C.P. (2005), Optimization of Fenton process for the treatment of landfill leachate, Journal of Hazardous Materials, 125, 166–174. https://doi.org/10.1016/j.jhazmat.2005.05.025.